COMPARISON OF MEASURED AND PREDICTED SOUND ABSORPTION PROPERTIES OF POLYESTER FIBRE INSULATION USING AN UNUSUAL PLANE WAVE TUBE

G Leembruggen Acoustic Directions, ICE Design Australia, University of Sydney Australia
D Gilfillan Gilfillan Soundwork, ICE Design Australia

1 INTRODUCTION

Measurements of the normal-incidence acoustic absorption properties of a number of samples were made using a long aluminium plane-wave tube and a single microphone. This use of a long plane-wave tube for acoustic absorption measurements is unusual, and was first described in the technical literature by Stevens and Vanderkooy (1).

The method using the long-tube and single microphone provides some worthwhile benefits over impedance tubes utilising two microphones that are generally used today:

- significantly reduced measurement times compared to the traditional two position methods,
- a considerably smaller volume of data to be acquired,
- only single channel instrumentation and one microphone is required
- excellent low frequency accuracy due to the elimination of mismatches in amplitude and phase between the two microphones

Knowledge of the normal incident absorption co-efficients is important for two reasons:

1) They indicate the trends of the measurements absorption co-efficients made in a reverberation chamber.
2) In speech and music spaces, sound waves that are normally-incident on some rear walls cause can problematic echoes. Absorption is one way of treating these echoes and therefore it is important to know the normal incidence absorption properties

2 TUBE OPERATION

2.1 Setup

The plane wave tube consists of a 6.6 m long aluminium tube of internal diameter 88 mm and 5.5 mm wall thickness. A 200 mm diameter loudspeaker is located at one end of the tube and produces sound over the frequency range of 30 Hz to 3 kHz. The acoustic absorption sample (sample under test) is fitted to the other end of the tube inside a removable assembly. So that the sample is visible in situ, it is mounted in a Perspex (Plexiglas) tube assembly, which also allows different air gaps to be provided behind the sample. This visibility allows visual confirmation that fibrous insulation is correctly mounted in the tube.

Figure 1 shows pictures of the tube, microphone and an insulation sample in situ. The loudspeaker is driven with a swept-sine wave signal, produced by WinMLS2004 acoustic analyser software. The resulting sound in the tube is picked up by a 12.5 mm Type 1 microphone that is inserted approximately half-way along the tube, and its output is processed by the WinMLS analyser.

The microphone's signal is mathematically de-convolved with the swept-sine wave signal to produce the impulse response of the tube system at the microphone.

Figure 1 Photos of the impedance tube

2.2 Acoustic Behaviour

The impulse response of the system as consists of a number of pulses that progressively decay over time, of which an example is given in Figure 2. The first pulse in that figure is due to the incident sound on the microphone, which has travelled directly along the tube from the loudspeaker. The second pulse is the sound that has been reflected from the material under test back towards the loudspeaker. A succession of pulses then follow, which are due to successive reflections of sound from the loudspeaker and material under test and show that the sound propagates forward and back along the tube until it decays away.

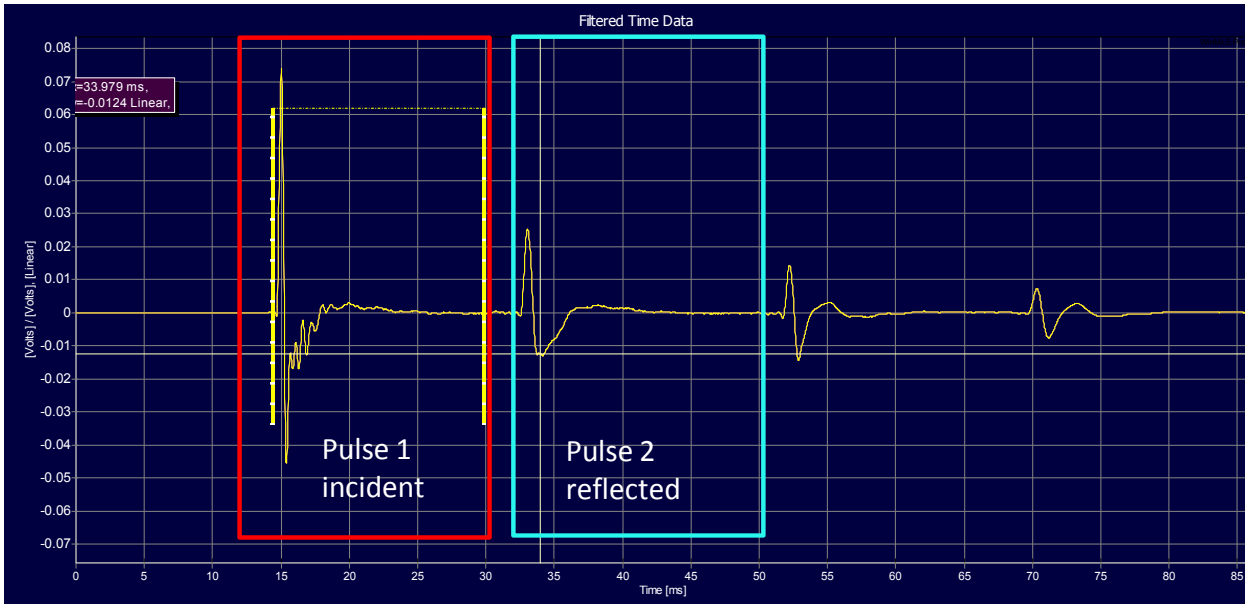

Figure 2 Example of an impulse response at the microphone

The following pulses in time-order are clearly visible in Figure 2:

i) the forward-travelling sound wave from the loudspeaker (Pulse 1) which is ultimately incident on the acoustic absorption material
ii) the backward travelling wave which is the reflection of Pulse 1 from the acoustic absorption material (Pulse 2)
iii) the forward-travelling sound wave which is the reflection of Pulse 2 from the loudspeaker
iv) subsequent reflection from the acoustic absorption material

The tube is sufficiently long to allow the incident pulse and reflected pulses to be sufficiently separated in time so that the decaying tail of the incident pulse does not intrude into the start of the reflected pulse.

Due to its diameter of 88 mm, the upper frequency limit of the tube is approximately 2.3 kHz, which is the frequency of the first transverse mode in the tube, after which plane wave behaviour ceases. At particular frequencies above 2.3 kHz, sound waves cease to propagate along the tube, and exist as circular standing-waves across the tube.

The time data of the impulse response is truncated or "windowed" using a Rectangular window to separate the incident sound from (Pulse 1) from the reflected sound (Pulse 2).

Using the Fast Fourier Transform (FFT), the frequency contents of the incident and reflected waves are found from the windowed time data. The ratio of the magnitude of the reflected sound and the incident sound is then found at each frequency, which provides the complex pressure reflection co-efficients as per Eq 1.

$$r = P_+ / P_- \qquad \text{Eq 1}$$

where:

r is the pressure reflection co-efficient

P_+ is the complex incident pressure reaching the microphone direct from the loudspeaker

P_+ is the complex reflected pressure reaching the microphone direct from the sample

From the magnitude of the pressure reflection co-efficient, the sound absorption co-efficient A is easily computed as per Eq 2.

.

$$A = 1 - r^2 \qquad \text{Eq 2}$$

The complex (real and imaginary) components of the acoustic impedance *Z* of the absorption material at each frequency can be also computed from the complex pressure reflection co-efficient at each frequency as per Eq 3.

$$Z = \frac{1 + r}{1 - r} \qquad \text{Eq 3}$$

2.3 Calibration of the Tube

To calibrate the tube system, a solid reflecting plate is fixed to the end of the tube and the pressure reflection co-efficient measured using Eq 1 . In this condition, the reflection co-efficient should equal 1.0 at all frequencies.

Differences from unity will be due to three main sources:

- overlap of the decaying incident pulse and the early part of the reflected pulse.
- errors associated with the windowing of the incident and reflected time data segments, which will occur if the pulse has not decayed to zero, when the window truncates (or "chops" through) the time data
- acoustic losses in the tube as the sound propagates along the tube.

2.3.1 Overlap and truncation errors

The tube system is sensitive at the lower frequencies to effects arising from the truncation of the time data by the windowing process. A change of 0.2 dB in the frequency response of the incident sound at 100 Hz due to a change in window length can cause a change of 0.035 in the absorption co-efficient at that frequency. To achieve a reflection co-efficient of 1 at 100 Hz, the shape of the incident pulse emitted by the loudspeaker was shaped by high-pass filtering to reduce its length, so that it has almost completely decayed by the time that the first reflected arrives at the microphone.

The selection of filter type is critical to the decay time, and the fastest decay time was achieved using a deep notch filter centred at 20 Hz with a wide bandwidth.

In addition to errors in the frequency response at low-frequencies arising from the truncation of a slowly decaying low frequency sound, response errors were also found to be caused by truncation though the ripples in the time-response caused by slowly decaying high-frequency sound, mainly at 2.3 kHz (the first resonant mode in the tube) although other frequencies were present . These components of the waveform were removed by inserting deep notch filters at specific frequencies and using a low-pass filter at 2.3 kHz, executed in WinMLS on the impulse response.

An expanded view of the impulse response at the microphone is given in Figure 3 and shows the incident sound and the first reflection. The reduction in i) the decay time at low frequencies and ii) the high frequency resonant mode due to the low frequency shaping and the high frequency filters being clearly visible.

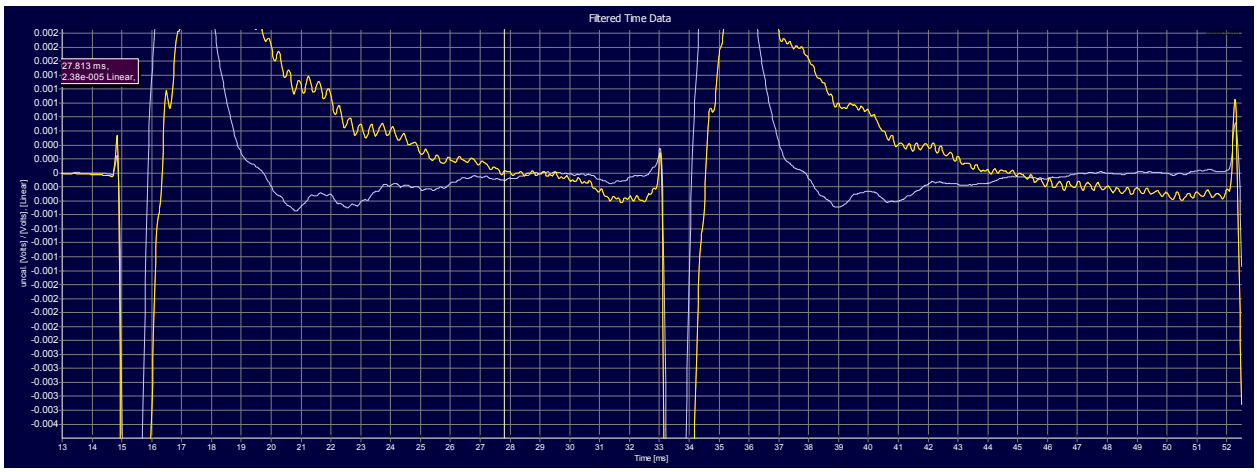

Figure 3 An impulse response of the tube system showing the incident and reflected sound. The yellow trace is without filtering applied to the loudspeaker, the white trace is with filtering.

2.3.2 Acoustic Losses

Losses in the tube (aside from reflection from the sample under test) are due to visco-thermal losses in the tube, which increase with frequency and are discussed in (2). The combination of Eq 4 from Stevens and Vanderkooy (1)(1) and Eq 5 from Chu (3) (3) (3) (3) give the predicted tube loss as a function of frequency.

$$r_{tube-loss} = e^{-2aL} \qquad \text{Eq 4}$$

with $$a = 0.0204\sqrt{(f\ /cD\ )} \qquad \text{Eq 5}$$

where *a* is the loss factor
L is the length of the tube in m
f is the frequency in Hz
c is the speed of sound in m/s
D is the diameter of the tube in m.

The losses predicted by Eq 5 were found to be higher than were measured for the tube and by curve-fitting, an alternative constant term in Eq 5 was found for our system. Figure 4 compares the measured losses, with the standard losses predicted by Eq 4 and the predicted losses when the 0.0204 constant in Eq 5 is replaced with a value of 0.0115.

The pressure reflection and absorption co-efficients for this corrected system are shown in Figure 5. The large spikes at 2.3 kHz indicate the presence of the first cross-mode in the tube.

Comparing these corrected reflection co-efficients to unity and the absorption co-efficient to zero, small differences still remain unaccounted for in this reference (or calibration) situation. The reciprocal of the reflection co-efficients are then used to provide an additional set of correction factors that normalise the reflection co-efficient at each frequency to unity and the absorption co-efficients to zero. These correction factors are applied to the reflected spectra of all subsequent measurements, and can be readily activated or de-activated.

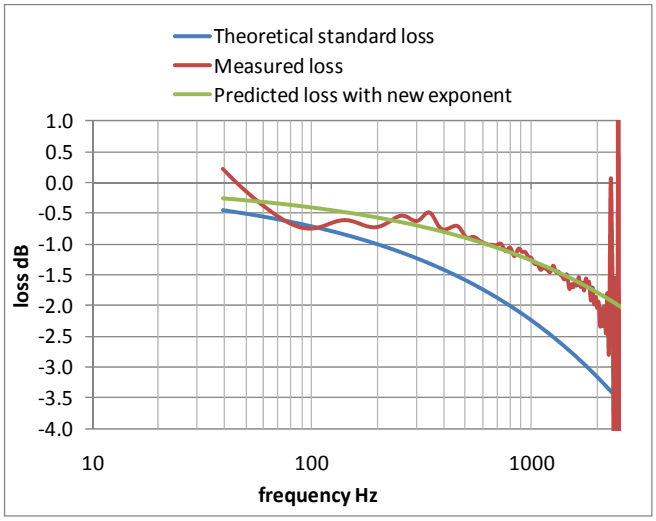

Figure 4 Comparison of measured and predicted losses in the plane wave tube.

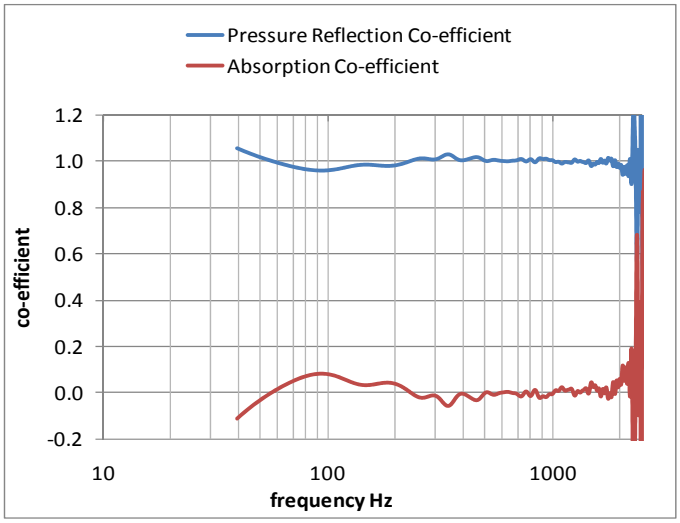

Figure 5 Pressure-reflection and absorption co-efficients with a solid end-of-tube and the predicted losses based on a constant term of 0.0115.

3 ACOUSTIC MODELS

A method to compute the acoustic properties of a combination of layers of different materials is outlined in (4) by Colam and Leembruggen (4). Guy (5) provides a good description of this method and shows how a system of many different layers can be modelled from knowledge of the individual layers' impedances and propagation constants and the continuity relationships between the layers. Cox and D'Antonio (6) also describe this method, which they term "transfer matrix method".

The model starts from a known terminating impedance and works through the multi-layer system calculating the transmission of sound through each layer according to the characteristic impedance and propagation constant of that layer. Equations of continuity are used at the junctions between individual layers. An example of how this is represented in the computational model is given in Figure 1. The acoustical output of the structure the terminating layer is a simple limp mass, which can take any value is. Subsequent layers of the multi-layer structure consist of air, porous material, limp masses or perforated panels. A plane wave is assumed to be normally incident to the system. The porous material can either be foam or fibrous material.

User inputs are the surface density of each mass, the perforation ratio, hole-diameter and material thickness of each perforated panel and the flow resistance and thickness of the foam or fibrous materials and any air gaps.

Outputs of the model are:

- normal incidence absorption coefficient
- random incidence absorption coefficient
- transmission loss
- phase of absorption co-efficient
- amplitude and phase of reflection coefficient
- magnitude and phase of the pressure at the incident face
- real and imaginary components of the resulting acoustic impedance

3.1 Model of Polyester Insulation

Prediction of the acoustic properties of polyester fibrous insulation was undertaken using the model of the characteristic acoustic impedance and complex propagation constant for polyester fibre insulation prepared by Garai and Pompoli (7). This model requires input of the flow resistivity of the insulation sample and assumes that the fibre diameter of the polyester lies within a specific range.

The model of Garai and Pompoli is based on polyester fibres with a circular section and a diameter ranging from 18 to 48 μm; with the mean fibre length is about 55 mm. Garai and Pompoli note that these values are considerably greater than those of glass wool fibres, which usually have diameters ranging between 1 and 10 μm. The polyester fibres are mainly organised in bi-dimensional layers parallel to the two main surfaces of the blanket.

Garai and Pompoli's predictive model for the normal-incidence sound absorption coefficient uses the well known Delany–Bazley power-law relations and Equations 3 to 6 and Table 3 in (7) give the exponents for the power-law equations particular to this model.

The manufacturer of the XHD range of polyester insulation tested in this work has confirmed that the fibre diameter of the insulation lies within the above range.

3.2 Model of Helmholtz Absorber

The model for the acoustic impedance of a perforated panel is taken from Lee and Swenson (8) with adjustments where appropriate by Maa (9). Maa suggests removal of the end-correction for the air mass in the holes, whenever K, given in Eq 6 exceeds 10. However, Lee and Swenson do not remove this end correction.

$$K = d\sqrt{2Pif\ \rho_0}/4v \qquad \text{Eq 6}$$

where: d is the diameter of the holes
f is the frequency
p_o = 1.21
v = viscosity of air = 1.9×10^{-5}

4 ABSORBERS TESTED

The absorption properties were measured for a range of absorber types:

- Polyester insulation of various grades and thicknesses with and without air spaces behind the insulation
- Perforated plates with polyester insulation behind
- Perforated plates without insulation behind the plate

Table 1 provides details of the absorption systems that were tested in the plane wave tube. Unless noted otherwise, the tube correction factors are the reciprocal of the reflection co-efficients shown in Figure 5. The R values in this table are the flow resistivities of the insulation samples.

The heating cycle used in the manufacture of some polyester insulation produces a slightly stiffer section on one side of the insulation. The additional stiffness progressively decreases over approximately 15 mm.

Test No	Type	Polyester Type & thickness	R MKS Rayls	Air gap behind system mm	Perforate structure	Comment	Figure
1	Insulation only	XHD100 95 mm	13770	nil	NA	NB XHD100 insulation seemed to be pulled apart slightly due to overuse. Crispy side towards end of tube.	Figure 6
2	Insulation only	XHD100 95 mm	13770	nil	NA	Stiffer side towards tube	Figure 7
3	Insulation + air gap	XHD100 95mm	13770	100 mm	NA	Stiffer side towards end of tube.	Figure 8
4	Insulation + air gap	XHD100	13770	100 mm	NA	Stiffer side towards tube.	Figure 9
5	Insulation only	AUT48/50 75mm	4574	nil	NA		Figure 10
6	Insulation only	AUT48/50 75mm	4574	25	NA		Figure 11

Test No	Type	Polyester Type & thickness	R MKS Rayls	Air gap behind system mm	Perforate structure	Comment	Figure
7	Insulation only	AUT48/50 75mm	4574	125	NA		Figure 12
8	Insulation only	XHD50 50 mm	14693	nil	NA	Stiffer side towards end of tube	Figure 13
9	Insulation only	XHD50 50mm	14693	nil	NA	Stiffer side towards end of tube, different sample from same batch, tested two months earlier.	Figure 14
10	Insulation + air gap	XHD50 50 mm	14693	50	NA	Stiffer side towards tube end.	Figure 15
11	Perforated panel only	NA	NA	100	1 mm thick plastic; 5.7% o/a; 1.4 mm dia. holes	Smooth holes Complete tube correction used.	Figure 16
						Exponential tube correction only.	Figure 17
12	Perforated panel + insulation	XHD50 50mm	14693	50	1 mm thick plastic; 5.7% o/a; 1.4 mm dia. holes smooth finish	Stiffer towards tube end, with Maa's correction >600 Hz.	Figure 18
13	Perforated panel only	NA	NA	100 mm	1.95 mm thick timber; 0.34% o/a; 0.7 mm dia. holes	Some roughness on holes.	Figure 19
14	Perforated panel only	NA	NA	100 mm	1.95 mm thick timber; 1.4% o/a; 1.5 mm dia. holes	Some roughness on holes.	Figure 20
15	Perforated panel + insulation	XHD100 100mm	13770	nil	1.95 mm thick timber; 1.4% o/a; 1.5 mm dia. holes Some roughness on holes	Without Maa's correction	Figure 21
						With Maa's correction>400Hz	Figure 22
16	Composite: Insulation A/ perforate/ insulation no2/ air gap	No1) 50 mm No 2) Articulated 44 mm	No1) 6222 No2) 23881	50 mm	1.95 mm thick timber; 1.4% o/a; 1.5 mm dia. holes	Without Maa's correction.	Figure 23
						With Maa's correction >400 Hz.	Figure 24
17	Perforated panel + insulation + air gap	XHD50 50 mm	14693	50 mm	9.3 mm thick MDF, 25% o/a 6.9 mm dia. holes	Stiffer side towards air gap. with Maa's correction >20 Hz.	Figure 25

Test No	Type	Polyester Type & thickness	R MKS Rayls	Air gap behind system mm	Perforate structure	Comment		Figure
18	Perforated panel + insulation + air gap	XHD50 50 mm	14693	50 mm	12.9 mm thick MDF, 22% o/a 9.9 mm dia. holes	Stiffer side towards air gap,	without Maa's correction	Figure 26
							with Maa's correction >20 Hz	Figure 27
19						Stiffer side towards tube		Figure 28
20	Perforated panel only + air gap	none		100 mm	9.6 mm thick MDF, 12% o/a, 4.8 mm dia. holes	full tube correction used		Figure 29
						Exponential tube correction only.		Figure 30
21	Perforated panel + insulation + air gap	XHD50 50 mm	14693	50 mm	9.6 mm thick MDF, 12% o/a, 4.8 mm dia. holes	With Maa's correction >50 Hz.		Figure 31
						Without Maa's correction.		Figure 32
22	Perforated panel + insulation + air gap	XHD50 50 mm	14693	50 mm	10 mm thick MDF, 23.5% o/a, 4.8 mm dia. holes	With Maa's correction >50 Hz.		Figure 33
23	Insulation only	WP30 30mm	14949	16 mm	NA	Stiffer side only slight and towards end.		Figure 34

Table 1 List of absorption systems tested in the plane wave tube

5 RESULTS.

5.1 Measured Results

The following figures show the results of the measurements identified in Section 4.

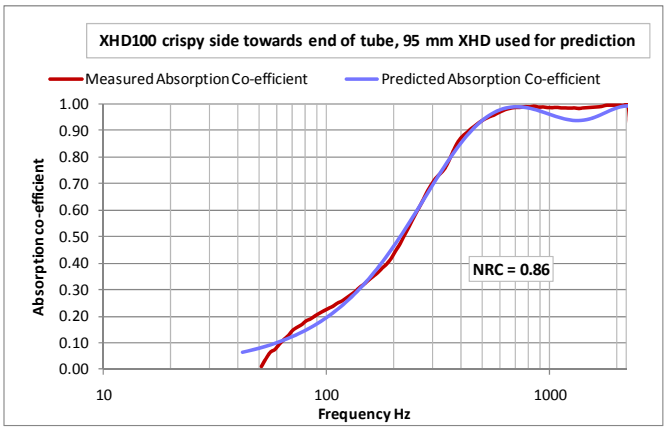

Figure 6
Test 1 XHD100 stiffer side towards end

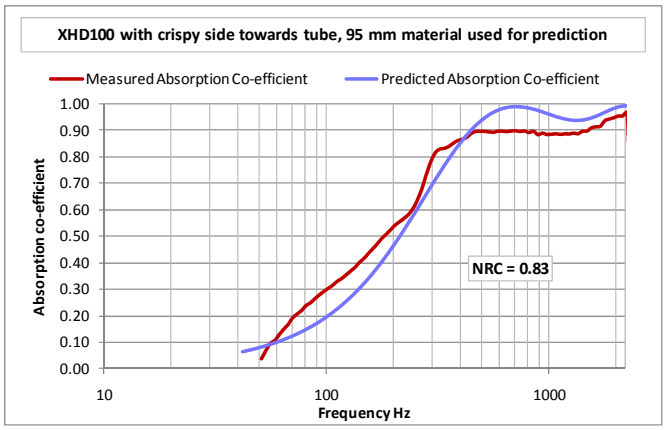

Figure 7
Test 2 XHD100 stiffer side towards tube

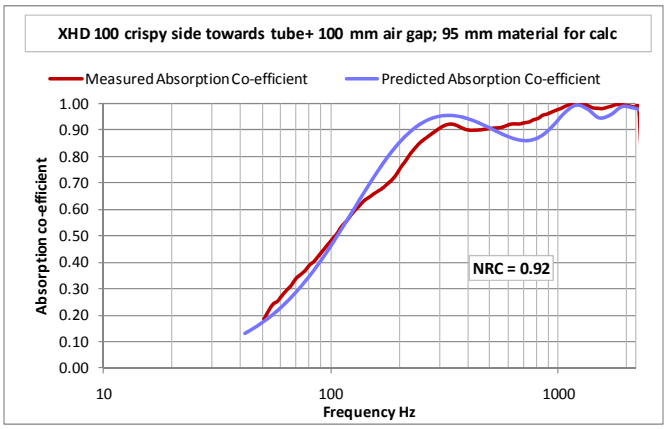

Figure 8

Test 3 XHD100 stiffer side towards end -100 mm air gap

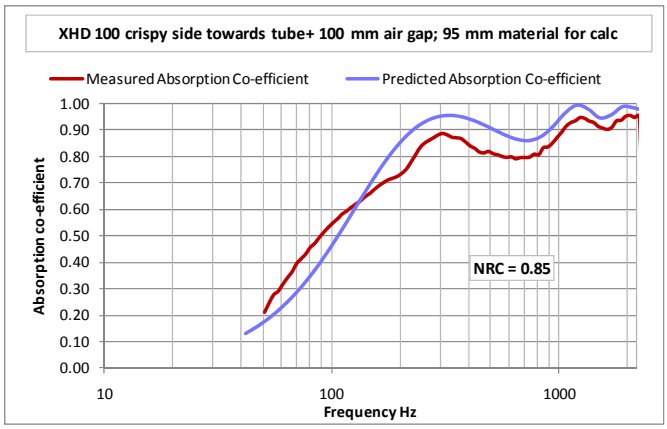

Figure 9

Test 4 XHD100 stiffer side towards tube - 100 mm air gap

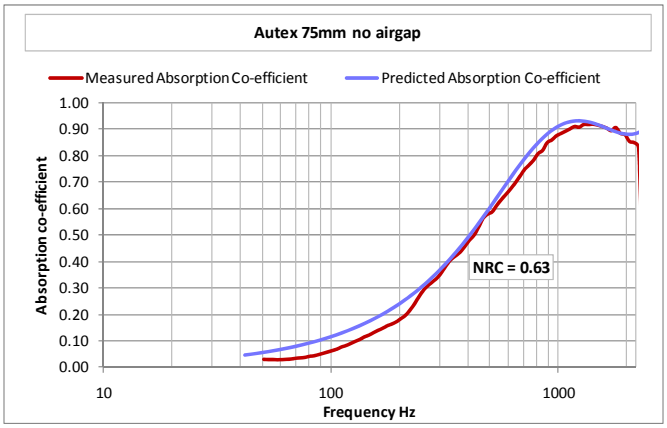

Figure 10

Test 5 Autex 48/50 65 mm no air gap

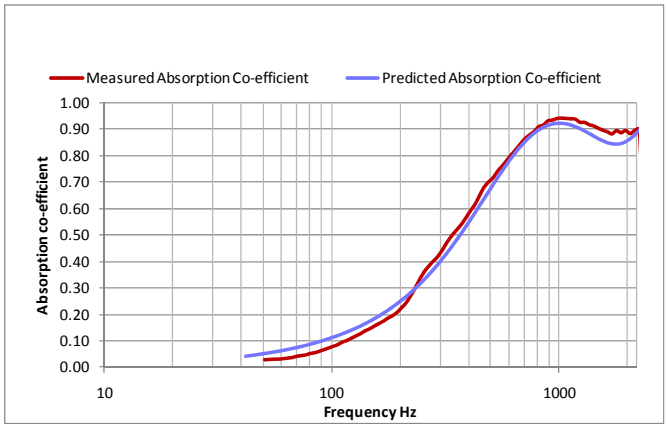

Figure 11

Test 6 Autex 48/50 65 mm 25 mm air gap

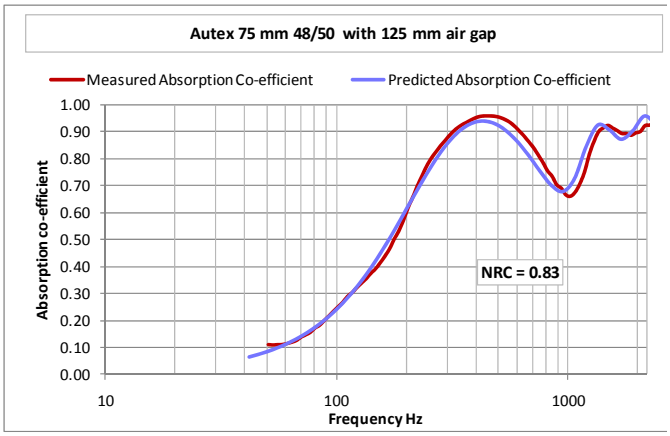

Figure 12

Test 7 Autex 48/50 65 mm 125 mm air gap

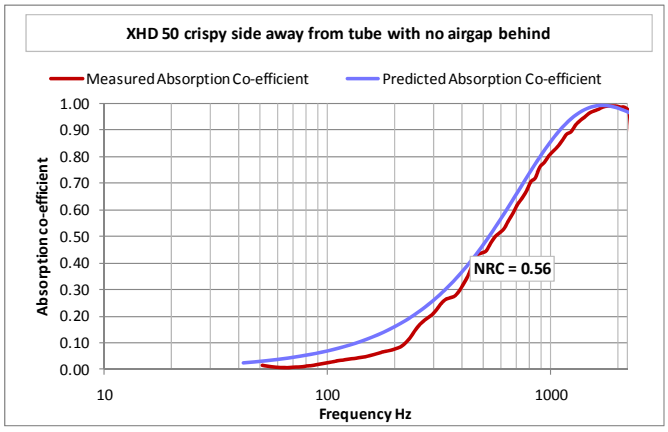

Figure 13

Test 8 XHD50 46 mm no air gap, stiffer side towards end of tube

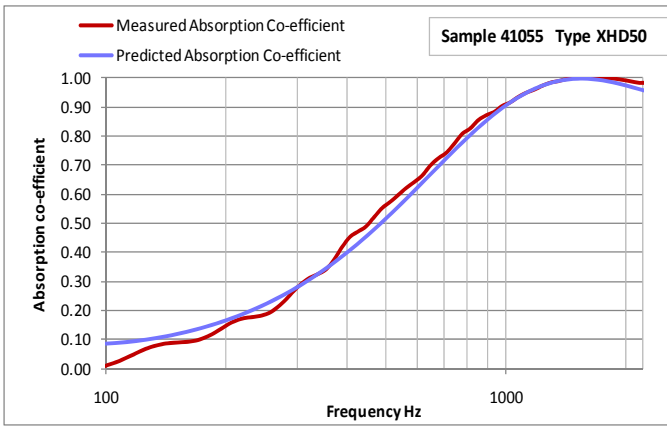

Figure 14

Test 9 XHD50 50mm different sample, same batch no air gap

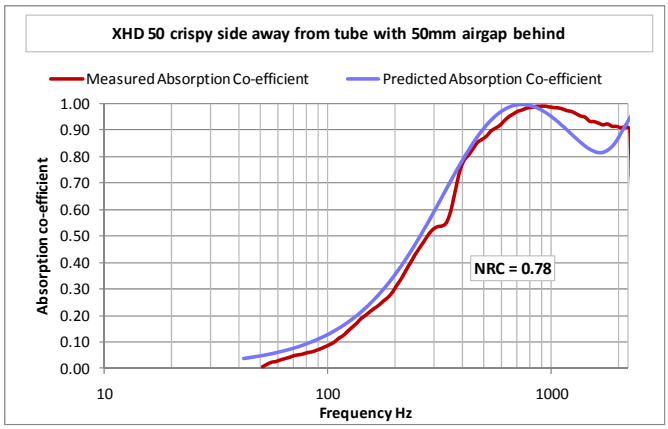

Figure 15

Test 10 XHD50 46 mm 50 mm air gap, stiffer side towards end of tube

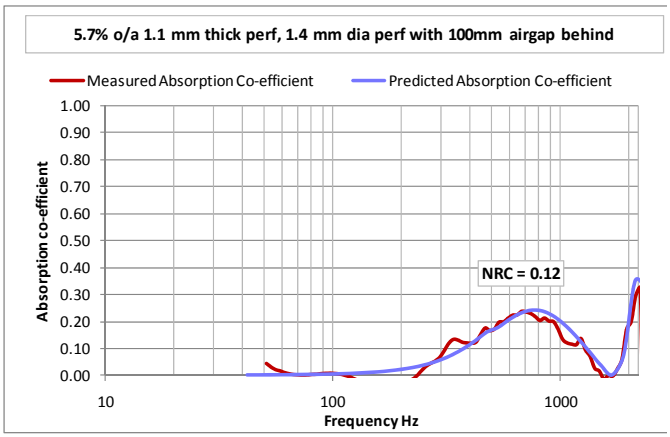

Figure 16

Test 11 Perf. 1.1 mm thick plastic ,5.7% o/a, 1.4 mm dia. holes with 100 mm air gap – full tube correction used

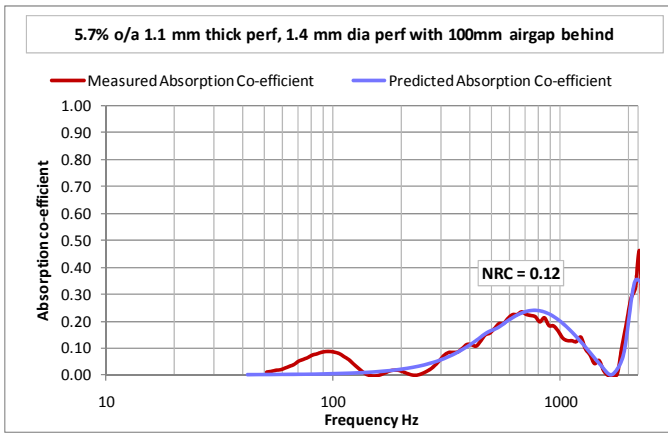

Figure 17

Test 11 Perf. 1.1 mm thick plastic, 5.7% o/a, 1.4 mm dia. holes with 100 mm air gap – exponential correction only

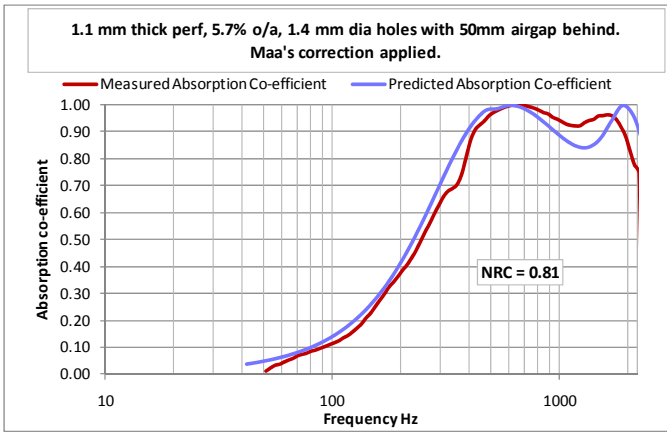

Figure 18

Test 12 Perf. 1.1 mm thick plastic, 5.7% o/a, 1.4 mm dia. holes with 46 mm XHD50 and 50 mm air gap, using Maa's correction

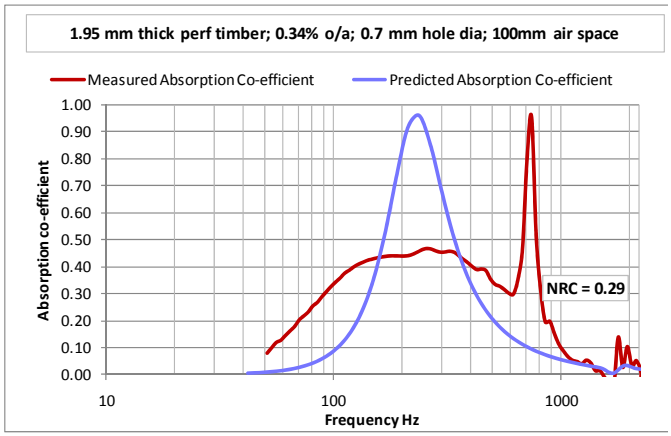

Figure 19

Test 13 Perf. 1.9 mm thick plywood, 0.34% o/a 0.7 mm holes with 100 mm air gap

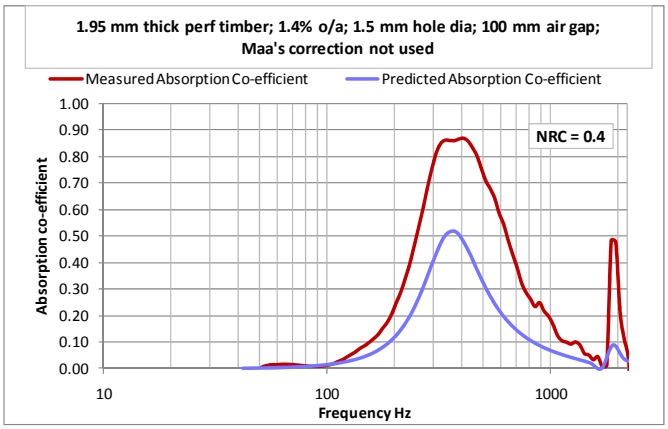

Figure 20

Test 14 Perf. 1.9 mm thick plywood,1.4% o/a 1.5 mm holes with 100 mm air gap

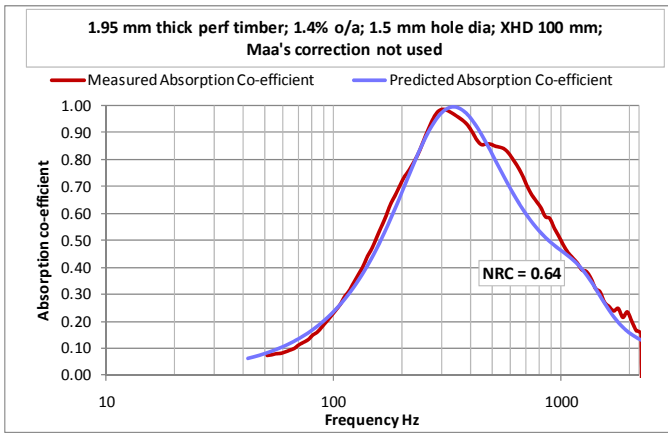

Figure 21

Test 15 Perf. 1.9 mm thick plywood, 1.4% o/a 1.5 mm holes with 100 mm air gap. Maa's correction not used.

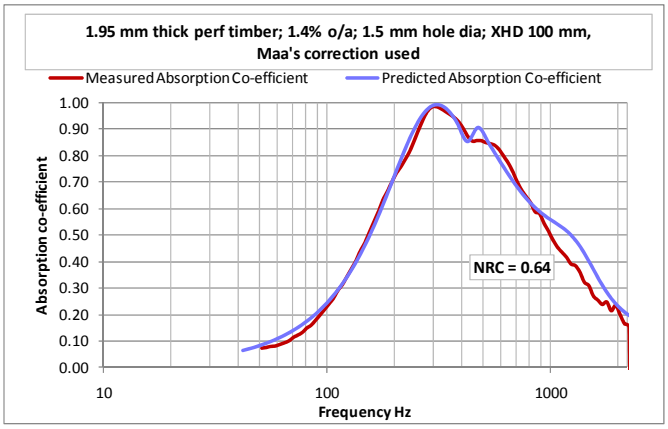

Figure 22

Test 15 Perf. 1.9 mm thick plywood,1.4% o/a 1.5 mm holes with XHD100 mm using Maa's correction

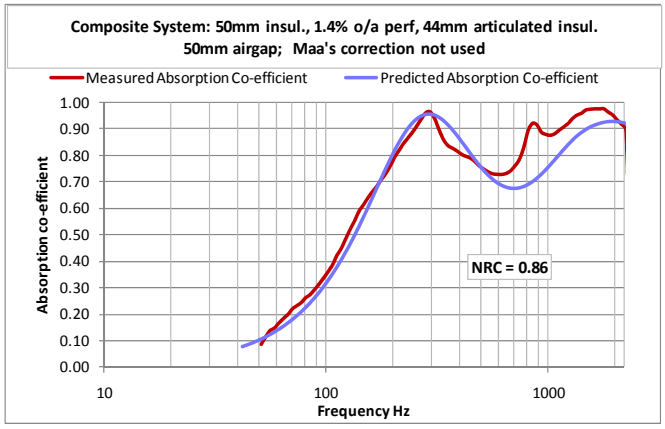

Figure 23

Test 16 Composite system without Maa's correction

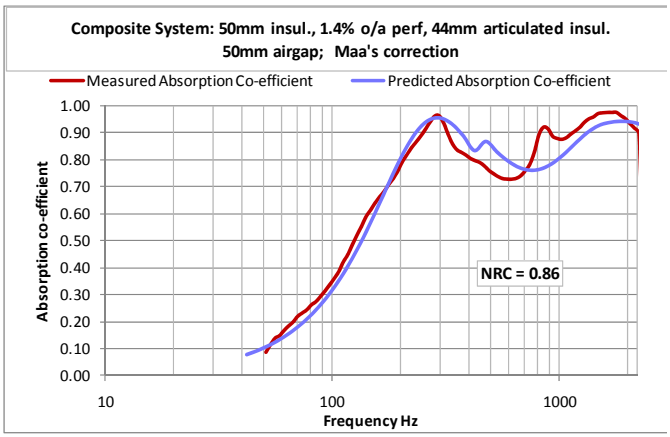

Figure 24

Test 16 Composite system using Maa's correction

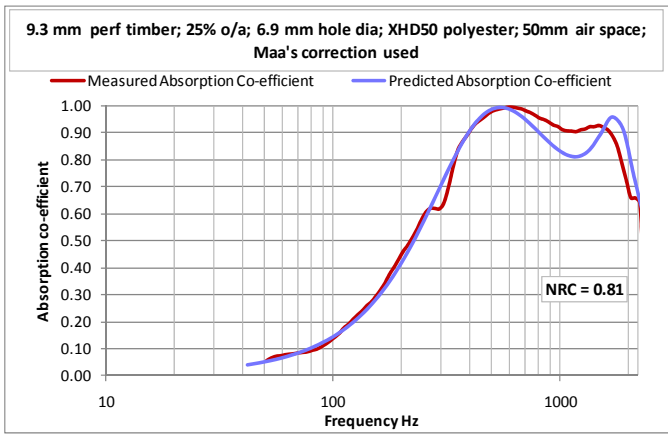

Figure 25

Test 17 Perf. 9.3 mm thick MDF, 6.9 mm dia. holes, 25% o/a with 50 mm XHD50 and 50 mm air gap – stiffer side towards air gap . Maa's correction used.

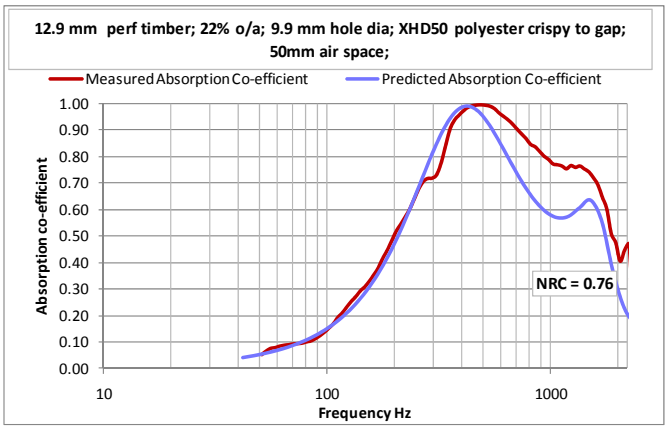

Figure 26

Test 18 Perf. 12.9 mm thick MDF, 9.9 mm dia. holes, 22% o/a with 50 mm XHD50 and 50 mm air gap – stiffer side towards air gap – Maa's correction not used

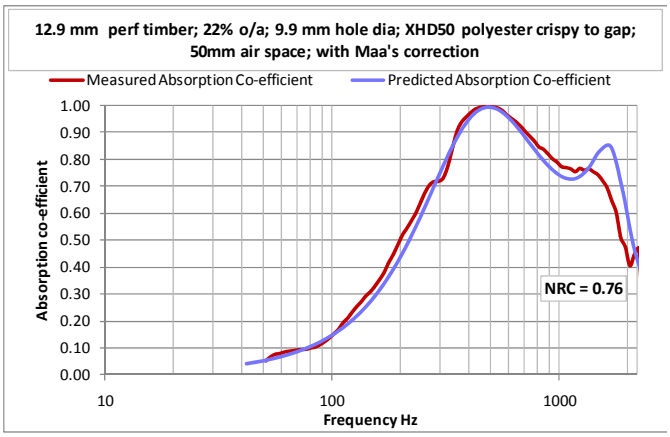

Figure 27

Test 18 Perf. 12.9 mm thick MDF, 9.9 mm dia. holes, 22% o/a with 50 mm XHD50 and 50 mm air gap – stiffer side towards air gap – Maa's correction used

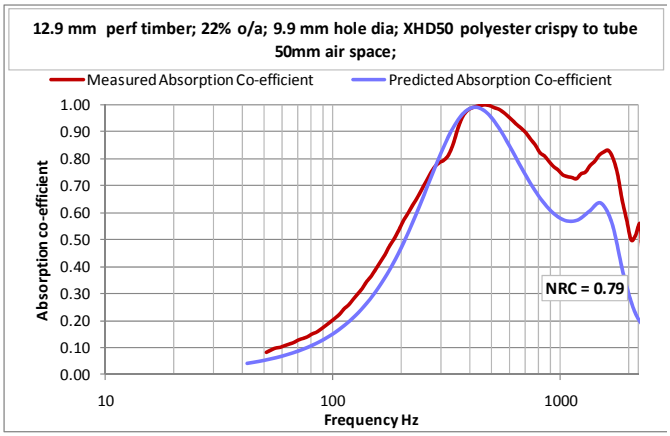

Figure 28

Test 19 Perf. 12.9 mm thick MDF, 9.9 mm dia. holes, 22% o/a with 50 mm XHD50 and 50 mm air gap – stiffer side towards tube

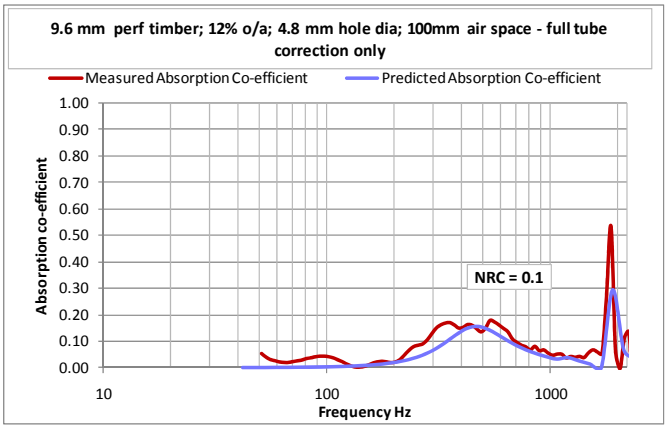

Figure 29

Test 20 Perf. 10 mm thick MDF, 4.8 mm dia. holes, 12% o/a with 100 mm air gap - full tube correction used.

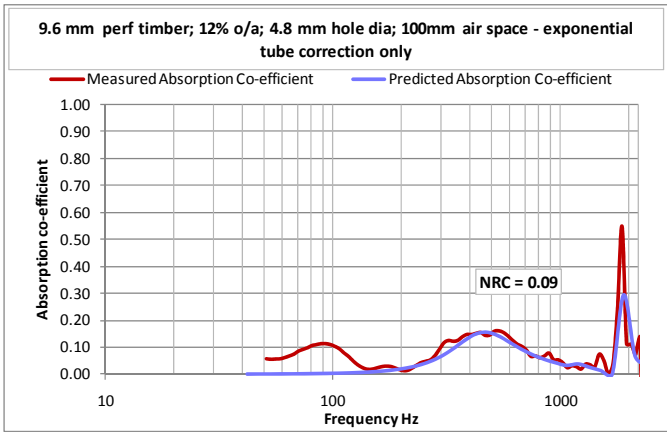

Figure 30

Test 20 Perf. 10 mm thick MDF, 4.8 mm dia. holes, 12% o/a with 100 mm air gap - exponential tube correction only

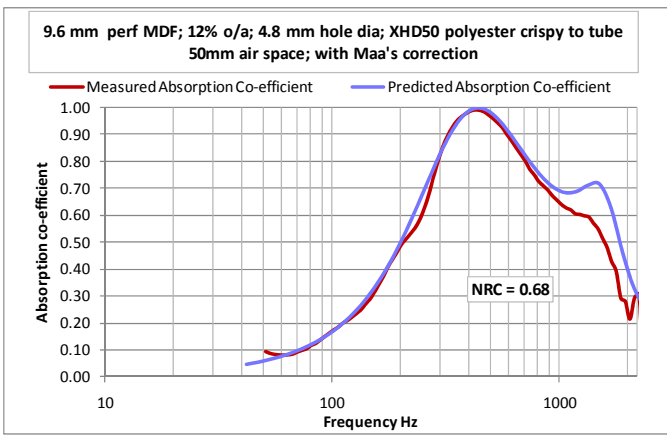

Figure 31

Test 21 Perf.9.6 mm thick MDF, 4.8 mm dia. holes, 12% o/a with XHD50 and 50 mm air gap.- with Maa's correction

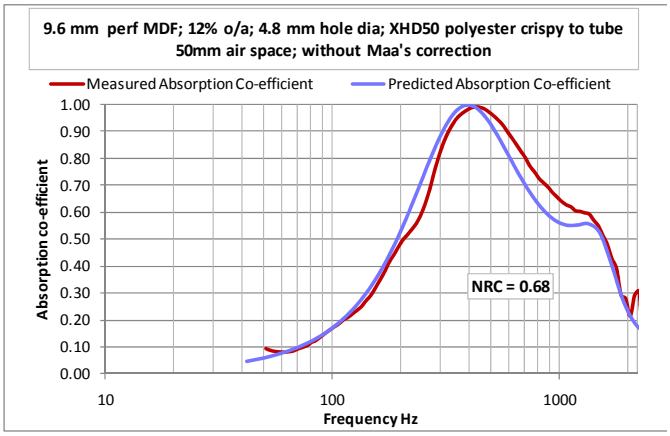

Figure 32

Test 21 Perf.10 mm thick MDF, 4.8 mm dia. holes, 12% o/a with XHD50 and 50 mm air gap.- without Maa's correction

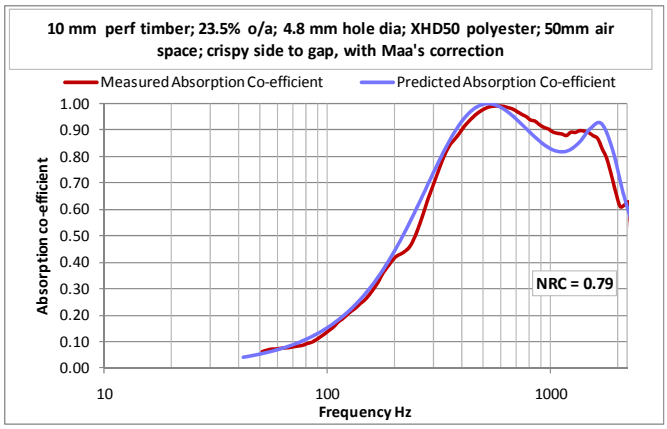

Figure 33

Test 22. Perf.10 mm thick MDF, 4.8 mm dia. holes, 23.5% o/a with XHD50 and 50 mm air gap.- with Maa's correction

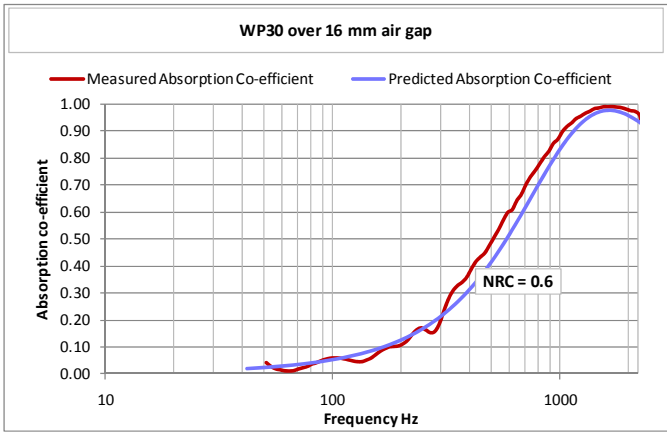

Figure 34

Test 23 WP30 30mm insulation with 16 mm air gap. Note the diameter of this sample was slightly oversize which resulted in slightly concave surface at the rear of the sample.

5.2 Analysis

The following trends are noted from the predictions and measurements:

- The predicted normal incidence absorption coefficients for the polyester insulation show good agreement with the measured incidence absorption coefficients when the stiffer side of the insulation faces towards the end of the tube; i.e away from the sound source.
- With the stiffer side of the insulation is mounted towards the sound source, the absorption at lower frequencies is higher than predicted and at higher frequencies, it is lower than predicted. We are wondering if these stiffer layers provide a small amount of membrane-type of absorption at low-frequencies, with the attendant loss of absorption at higher frequencies resulting from that mass-like structure.
- Many of the predictions show a dip in absorption in the frequency range of 1 kHz to 2 kHz, which is due to damped mode between the insulation and the solid end of the tube. The depth of these predicted dips is generally not mirrored in the measurements, indicating a higher-than-predicted absorption. However, there were cases such as Figure 12 and

Figure 16 in which the measured absorptions closely match the predicted in the 1 kHz to 2 kHz range.

- The thickness of the sample when located in the tube was not necessarily exactly the nominal thickness, due to slight compression effects. When attempting to match the measured and predicted absorption properties, we found that changes as small as 5mm in the thickness of the insulation used for predictions could cause important differences in the absorption versus frequency characteristic. In this context, the prediction model uses the actual thickness in the tube, with the flow resistivity adjusted accordingly.
- Some of the measurement results may have been affected by the constraint applied by the tube walls on the circumferential edge of the insulation. This effect is discussed in (10).
- Normalisation of the tube's innate response, i.e. with a fully reflecting end was undertaken in two stages. Stage 1 was to select a generic value for losses, while Stage 2 was to normalise the residual errors to a reflection co-efficient value of 1. The results suggest that the use of the Stage 1 method of normalisation is best applied down to 130 Hz, and below 130 Hz, the Stage 2 method should be used.
- The model for the Helmholtz system based on the perforated panels with 10 mm holes without insulation agrees with the measured result. But as the hole-diameter reduces, the model becomes less accurate. With a hole-diameter of 1.5 mm, the predicted absorption is less than measured, but with a diameter of 0.7 mm, the predicted absorption was much greater than measured. We conclude that the terms in the equations describing losses in the holes need refining, or that manufacturing techniques are important parameters to the acoustic losses.
- In the range of Helmholtz absorbers that we tested, when Maa's recommended correction was implemented in the predictions, there was important improvement in agreement between measured and predicted absorptions. This improvement was not systematic .
- There is a considerable change in some predictions when the Maa correction kicks in; a good example is seen in Figure 22 for Test 15 in which there is a bump at 400 Hz followed by a widening of the main absorption peak. Interestingly, the measured absorption also shows a small plateau in the region of 400 Hz to 500 Hz.

6 CONCLUSIONS

- When the model of Garai and Pompoli is used to predict the normal incidence absorption of systems using polyester insulation, the predicted absorption vs frequency characteristic matches our measured results quite well. (Note that due to the size of the impedance tube, our tests were only conducted up to 2 kHz.
- There was good agreement between measured and prediction absorption up to 1 kHz. For materials with higher flow resistivity, the agreement between measured and predicted was not as good between 1 and 2 kHz as below 1 kHz. With low flow-resistivity insulation or no insulation, the agreement was good up to the limit of the tube.
- This mismatch at the higher flow resistivities may indicate a need for refinements to the acoustic model. However, some of the mismatches may also be due to the way the insulation was mounted in the tube, as it was difficult to make the insulation evenly cover the tube along the length of the sample.
- Some of the measurement results may have been affected by the constraint applied by the tube walls on the circumferential edge of the insulation.
- The transfer matrix method of predicting the normally-incident sound absorption properties of a system using specific layers of masses, insulation, and air gaps can produce predicted absorptions that are close to measured. This method can provide important data to enable the design of such absorbers. The model of Garai and Pompoli for polyester insulation is

an important component of this method. The correction recommended by Maa for the resistive losses in the holes of a perforated panel results in a generally improved agreement between measured and predicted absorptions, when taken as a whole, but with worse agreement in some situations.

- The plane-wave tube is a useful adjunct to the acoustician's toolbox, and is able to readily provide absorption data for normally-incident absorption situations and to assist development of products for ultimate testing in reverberation chambers.
- A longer tube would allow absorption measurements down to lower frequencies, while a shorter, narrow tube would provide measurements above 2 kHz. The results of these tubes could be readily grafted together.

7 ACKNOWLEDGEMENTS

We gratefully acknowledge the assistance of the following organisations for this work:

- Acoustic Studio Pty Ltd for measurement of the flow resistivities of the insulation
- Martini Industries Pty Ltd for the supply of the XHD and WP polyester insulation
- Decor Systems Australasia for the supply of most of the perforated panels

8 REFERENCES

1. R. D. Stevens and J. Vanderkooy. A Novel Single-Microphone Method of Measuring Acoustical Impedance in a Tube. *115th AES Convention Paper 5901.* 2000.
2. J. W. van Honschoten, H-E. de Bree, F. J. M. van Eerden, and G. J. M. Krijnen. The Influence of Viscothermal Effects on Calibration Measurements in a Tube. *109th AES Convention Paper 5182.* 2000.
3. W.T. Chu . Extension of the two-microphone transfer function method for impedance tube measurements. *Journal of the Acoustical Society of America.* 1986, Vol. 80, 1.
4. S. Colam, G. Leembruggen. Analysis And Design Of Acoustic Absorbers And Low Frequency Transmission Loss. 2003 IOA Reproduced Sound Conference 19.
5. R. Guy. A Preliminary Study Model for the Absorption or Transmission of Sound in Multi-Layer Systems. *Noise Control Engineering Journal.* 1989, Vols. 33,, No. 3 pp. 117 - 123.
6. T. Cox & P. D'Antonio. *Acoustic Absorbers and Diffusers: Theory, Design, And Application.* s.l. : Taylor & Francis Group, 2004.
7. M. Garai, F. Pompoli. A simple empirical model of polyester fibre materials for acoustical applications. *Applied Acoustics.* (2005), Vol. 66, 1383–1398.
8. J. Lee, G. Swenson. Compact Sound Absorbers for Low Frequencies. *Noise Control Engineering Journal,.* 1992, Vols. 38,, No. 3, pp. 109 - 117.
9. D.Y Maa. Potential of Microperforated Panel Absorber. *Journal of the Acoustical Society of America.* 1998, Vol. 104, No. 5 (November), pp. 2861 - 2866.
10. B H. Song, J.S. Boltona, Y. J. Kang. Effect of circumferential edge constraint on the acoustical properties of glass fiber materials. *J. Acoust. Soc. Am. .* Vol. 110, 6 December 2001.